ORIGINAL RESEARCH

In vitro biocompatibility of calcined mesoporous silica particles and fetal blood cells

Mohammed T Al Samri[1,*]
Ankush V Biradar[2,3,*]
Ahmed R Alsuwaidi[1]
Ghazala Balhaj[1]
Suleiman Al-Hammadi[1]
Safa Shehab[4]
Suhail Al-Salam[5]
Saeed Tariq[4]
Thachillath Pramathan[1]
Sheela Benedict[1]
Tewodros Asefa[2,3]
Abdul-Kader Souid[1]

[1]Department of Pediatrics, Abu Dhabi, United Arab Emirates; [2]Department of Chemistry and Chemical Biology, [3]Department of Chemical Engineering and Biochemical Engineering, Rutgers, The State University of New Jersey, Piscataway, NJ, USA; [4]Department of Anatomy, Faculty of Medicine and Health Sciences, United Arab Emirates University, Al Ain, Abu Dhabi; [5]Department of Pathology Faculty of Medicine and Health Sciences, United Arab Emirates University, Al ain, Abu Dhabi, United Arab Emirates

*These authors contributed equally to this work

Correspondence: Abdul-Kader Souid
Department of Pediatrics, Faculty of Medicine and Health Sciences, United Arab Emirates University, Al Ain, Abu Dhabi, 17666, United Arab Emirates
Tel +971 3 713 7429
Fax +9 71 3 767 2022
Email asouid@uaeu.ac.ae

Background: The biocompatibility of two forms of calcined mesoporous silica particles, labeled as MCM41-cal and SBA15-cal, with fetal blood mononuclear cells was assessed in vitro.

Methods and results: Fetal mononuclear cells were isolated from umbilical cord blood and exposed to 0.5 mg/mL of MCM41-cal or SBA15-cal for several hours. Transmission electron micrographs confirmed the presence of particles in the cytosol of macrophages, neutrophils, and lymphocytes without noticeable damage to the cellular organelles. The particles (especially MCM41-cal) were in close proximity to plasma, and nuclear and mitochondrial membranes. Biocompatibility was assessed by a functional assay that measured cellular respiration, ie, mitochondrial O_2 consumption. The rate of respiration (k_c, in μM O_2 per minute per 10^7 cells) for untreated cells was 0.42 ± 0.16 (n = 10), for cells treated with MCM41-cal was 0.39 ± 0.22 (n = 5, $P > 0.966$) and for cells treated with SBA15-cal was 0.44 ± 0.13 (n = 5, $P > 0.981$).

Conclusion: The results show reasonable biocompatibility of MCM41-cal and SBA15-cal in fetal blood mononuclear cells. Future studies are needed to determine the potential of collecting fetal cells from a fetus or neonate, loading the cells in vitro with therapeutic MCM41-cal or SBA15-cal, and reinfusing them into the fetus or neonate.

Keywords: mesoporous silica, nanomaterials, biocompatibility, bioenergetics, in vitro, fetal cells

Introduction

The term "nanotoxicology" refers to the discipline that studies structural and functional cellular derangements produced by particles 1–100 nm in size.[1,2] For example, treatment of lymphocytes with multiwalled carbon nanotubes (20–40 nm) induces apoptosis.[3] Further, some silica and water-soluble fullerene nanoparticles are reported to extract electrons from the mitochondrial respiratory chain, producing deleterious oxidative damage.[4–7] Many of the toxic properties exhibited by nanomaterials are associated with ultrastructural alterations within the cell.[8] Not surprisingly, these changes are dependent on the dose, size, shape, surface area, aggregation, and surface functional conjugation of the materials.

Interestingly, a wide variety of other nanostructured and microstructured materials have been shown to be biocompatible with various cells and tissues.[9–11] Many of them have also been investigated for biological and medical applications, such as drug delivery[9,10,12–17] and bioimaging.[8] A few types of nanoparticles have shown good promise and have been commercialized as smart delivery vehicles or diagnostic agents for various diseases. However, comprehensive in vitro studies of the effects of nanomaterials and micromaterials on fetal cells are still necessary before scientists and biomedical engineers can extend their use to the fetus and the neonate.

MCM-41 and SBA-15 mesoporous silica particles have a high surface area and monodispersed nanometer pores, typically about 2 nm and 8 nm in diameter, respectively.[18,19] They are synthesized by supramolecular self-assembly of alkoxysilanes with cetyltrimethylammonium bromide (CTAB) surfactant or Pluronic 123 triblock copolymer templates. Removal of these organic templates is responsible for the formation of mesopores in the materials. Because of their attractive structures, with high surface area and pore volume, both MCM-41 and SBA-15 have been widely studied for delivery of small molecules, small interfering RNAs, and genes.[9,10,12–17] Their biological properties (toxicity or biocompatibility) have also been widely investigated. Interestingly, contradictory results have been documented in a few studies. For instance, a recent in vivo study suggested efficient uptake and biocompatibility of mesoporous silica nanospheres in murine pneumatocytes and mesothelioma cells.[20] In contrast, toxicity of MCM-41 and SBA-15 in mesothelial cells has been reported, eg, intraperitoneal and intravenous injections of either particle produced pulmonary thromboembolic events.[21]

Differences in dose, surface area, surface charge, pore diameter, residual reagents, and templates on the materials, as well as route of administration, have all been implicated as potential causes of conflicting results. For instance, differences in cellular bioenergetics, cellular uptake, distribution, and other adverse effects have been observed with a variety of mesoporous silica particles prepared by different synthetic methods.[4,15,17,20,21]

In addition, the methods used for removing organic templates from mesoporous materials may produce mesoporous materials with different properties, as was discovered recently.[22] Generally, two methods are used to remove the organic templates from these mesoporous materials, ie, high-temperature calcination in air or simple solvent-washing (extraction). In our recent studies, we showed that MCM41-cal or SBA15-cal prepared by calcination did not inhibit cellular bioenergetics and were biocompatible in murine liver, lung, pancreas, kidney, and spleen tissue.[23] The particles also did not alter cellular configurations or organelles. However, their solvent-extracted counterparts inhibited pneumatocyte respiration. The differences between calcined and solvent-extracted mesoporous silicas were attributed to the lack of residual organic materials in the calcined particles, as well as to the less surface density of silanol (Si-OH) groups, which are often implicated in the toxicity of silicas.[24,25]

The present study investigated MCM41-cal and SBA15-cal particles in fetal mononuclear cells collected from umbilical cord blood immediately after delivery. The data overall show

reasonable biocompatibility of calcined mesoporous silica particles in fetal mononuclear blood cells.

Materials and methods
Reagents

A Pd(II) complex of *meso*-tetra-(4-sulfonatophenyl)-tetrabenzoporphyrin was obtained from Porphyrin Products (Logan, UT). RPMI-1640 cell culture medium was sourced from Mediatech (Herndon, VA). Glucose oxidase (powder from *Aspergillus niger*), D (+) glucose anhydrous, Histopaque-1077, CTAB, tetraethyl orthosilicate, fluorescein 5(6)-isothiocyanate, and the remaining reagents were purchased from Sigma-Aldrich (St Louis, MO). Poly(ethylene oxide)-*block*-poly(butylene oxide)-*block*-poly(ethylene oxide) (Pluronic 123) $[(PEO)_{20}(PPO)_{70}(PEO)_{20}]$ was purchased from BASF (Florham Park, NJ).

Solutions

Pd phosphor solution (2.5 mg/mL = 2 mM) was prepared in dH_2O and stored at $-20°C$. Glucose oxidase solution was prepared in dH_2O (10 mg/mL) and stored at $-20°C$. NaCN solution (1.0 M) was prepared in dH_2O; the pH was adjusted to about 7.0 with 12 N HCl and the solution was stored at $-20°C$. Phosphate-buffered saline with glucose (137 mM NaCl, 2.7 mM KCl, 4.3 mM Na_2HPO_4, 1.4 mM KH_2PO_4, and 5 mM glucose; pH 7.4) was stored in the refrigerator for one week.

Isolation of peripheral blood mononuclear cells

Blood (5–10 mL) was collected from the umbilical cord immediately following delivery in heparinized syringes and processed within one hour of collection. Samples were diluted with an equal volume of phosphate-buffered saline plus 10 mM glucose and gently layered on top of 10 mL of Histopaque-1077. The mixtures were centrifuged at 15°C and 400 g for 30 minutes. The peripheral blood mononuclear cells collected were diluted with phosphate-buffered saline plus 10 mM glucose and centrifuged at 15°C and 400 g for 15 minutes. The pellets were suspended in phosphate-buffered saline plus 10 mM glucose, 3 μM Pd phosphor, and 0.5% fat-free bovine serum albumin. Cell count and viability were determined by light microscopy, using a hemocytometer under standard trypan blue staining conditions. Collection of blood from the umbilical cords was approved by the Institutional Review Board for Protection of Human Subjects. Informed consent was obtained for each participating subject.

Synthesis of MCM41-cal

MCM41 was synthesized as described previously.[18] Typically, CTAB (4.0 g, 1.1 mmol) was dissolved in Millipore water (960 mL) and 2.0 m NaOH solution (14 mL). After moderate stirring of the solution at 80°C for 30 minutes, tetraethyl orthosilicate (101.2 mmol) was added. The resulting solution was stirred for another 2 hours at 80°C. The hot solution was then filtered and the solid product was washed with Millipore water (4 × 80 mL), followed by ethanol (4 × 80 mL), and then dried in an oven at 80°C. This resulted in as-synthesized mesostructured MCM41. The CTAB surfactant template from the as-synthesized

MCM41 was removed by calcination. Two grams of the as-synthesized MCM41 sample was calcined in a tube furnace at 550°C for 6 hours under airflow (the temperature was raised from room temperature to 550°C at a rate of 10°C per minute). This produced calcined MCM41 (labeled here as MCM41-cal). The properties of the particles are shown in Figure 1 and Table 1.

Synthesis of SBA15-cal

SBA15 was prepared as reported previously[19] with slight modification. A solution containing 12 g of Pluronic 123, 313 g Millipore water, and 72 g HCl (36 wt%) was prepared
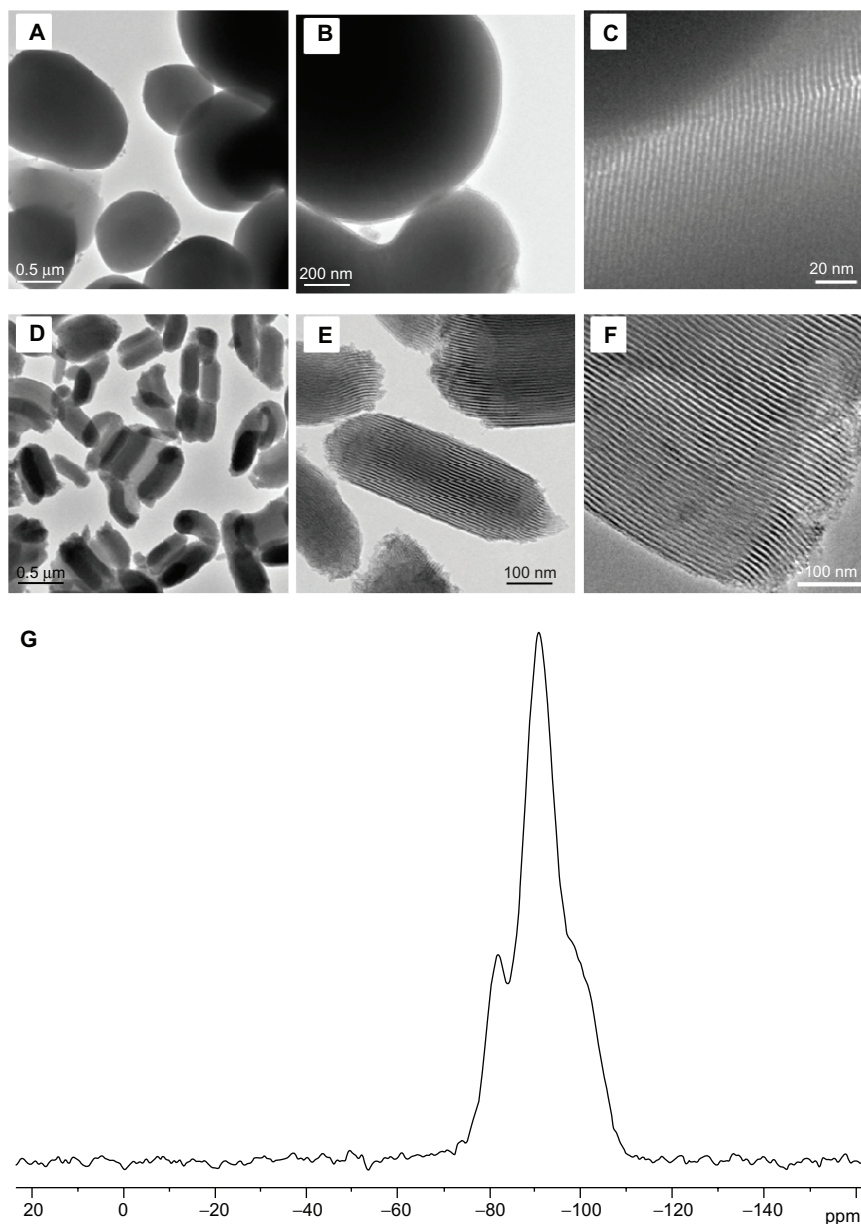

Figure 1 Large area and magnified transmission electron microscopic images of (**A–C**) MCM41-cal and (**D–F**) SBA15-cal materials. (**G**) Representative ^{29}Si magic angle spinning solid-state nuclear magnetic resonance spectra of MCM41-cal material.

Table 1 Physical characteristics of MCM41-cal and SBA15-cal

Analysis/characterization	MCM41-cal	SBA15-cal
Transmission electron microscopy	Regular spherical/oval-shaped, 300–1000 nm diameter	Irregular shapes and sizes, mostly rods of 500 nm diameter and about 1000 nm long
Powder x-ray diffraction	Highly ordered mesostructures with sharp low-angle Bragg reflection; lattice spacing of ~44 Å	Highly ordered mesostructures with sharp low-angle Bragg reflection; lattice spacing of about 106 Å
Nitrogen gas adsorption	Type IV isotherms with steep capillary condensation; large surface area and uniform size mesopores	Type IV isotherms with steep capillary condensations; large surface areas and uniform size mesopore
^{13}C CP-MAS solid-state NMR[1]	No residual CTAB surfactant (template); no residual ethoxy groups from TEOS	No residual Pluronic P123 block copolymer templates; no residual ethoxy groups from TEOS
Elemental analysis	No residual CTAB	No residual Pluronic P123 block copolymer templates
^{29}Si MAS solid-state NMR	Significant Q4 silicon sites centered at 110 ppm; little Q3 and Q2 centered at 101 and 91 ppm, respectively	Significant Q4 silicon sites centered at 110; significant Q3 centered at 101 ppm and some Q1 centered at 91 ppm
Nitrogen gas adsorption	BET surface area approximately 1290 m^2/g; mean BJH pore diameter^2 about 28 Å	BET surface area about 955 m^2/g; mean BJH pore diameter^2 about 59 Å

Abbreviations: BET, Brunauer-Emmett-Teller; BJH, Barrett-Joyner-Halenda; CP-MAS, cross-polarization magic angle spinning; CTAB, cetryltrimethylammonium bromide; NMR, nuclear magnetic resonance; TEOS, tetraethyl orthosilicate.

and stirred vigorously at 40°C until the Pluronic template had dissolved. Tetraethyl orthosilicate 25.6 g was then added, and the solution was stirred at 45°C for 24 hours. After keeping it under static condition in the oven at 80°C for 24 hours, the solution was filtered. The solid material was washed with Millipore water and ethanol (3 × 80 mL) and dried under ambient conditions to produce as-synthesized SBA15 particles. The Pluronic 123 template from the as-synthesized SBA15 sample was removed by calcination as described above, and the resulting mesoporous sample was labeled as SBA15-cal. The particles were stored at 25°C in a vacuum desiccator until further use. The properties of the particles are shown in Figure 1 and Table 1.

Oxygen measurement

A phosphorescence analyzer that measures dissolved O_2 in solutions as a function of time was used to determine the rate of cellular respiration. This method is based on the principle of O_2 quenching the phosphorescence of palladium phosphor. The Pd (II) derivative of *meso*-tetra-(4-sulfonatophenyl)-tetrabenzoporphyrin has an absorption maximum at 625 nm and a phosphorescence emission maximum at 800 nm. Samples were exposed to light flashes (10 per second) from a pulsed light-emitting diode array with a peak output at 625 nm (OTL630A-5-10-66-E, Opto Technology Inc, Wheeling, IL). Emitted phosphorescent light was detected by a Hamamatsu photomultiplier tube after first passing the samples through a wide band interference filter centered at 800 nm. Amplified phosphorescence was digitized at 1–2 MHz using an analog/digital converter (PCI-DAS 4020/12 I/O board) with 1–20 MHz outputs (Computer Boards Inc, Mansfield, MA).

Pulses were captured at 0.1–4.0 MHz, using a software program developed for this use.

The program was developed using Microsoft Visual Basic 6, Microsoft Access Database 2007, and Universal Library components. This allowed direct reading from the PCI-DAS 4020/12 I/O Board. The software included a relational database that stores experiments, pulses, and pulse metadata, including slopes. Pulse detection was accomplished by finding 10 phosphorescence intensities above 1.0 volt. Peak detection was accomplished by finding the highest 10% data points of a pulse, and then choosing the one in the group that was closest to the pulse decay curve. Depending on the sample rate, a minimum number of data points per pulse was set and used as a cutoff to remove invalid pulses with too few data points.

The phosphorescence decay rate ($1/\tau$) was characterized by a single exponential, $I = Ae^{-t/\tau}$, where I = Pd phosphor phosphorescence intensity. The values of $1/\tau$ were linear with dissolved O_2: $1/\tau = 1/\tau^o + k_q[O_2]$, where $1/\tau$ = the phosphorescence decay rate in the presence of O_2, $1/\tau^o$ = the phosphorescence decay rate in the absence of O_2, and k_q = the second-order O_2 quenching rate constant in sec^{-1} μM^{-1}.

Cellular respiration was measured at 37°C in 1 mL sealed vials. Mixing was carried out with the aid of parylene-coated stirring bars. The respiratory substrates were endogenous metabolic fuels supplemented with glucose. In cell suspensions sealed from air, $[O_2]$ decreased linearly with time, indicating that the kinetics of mitochondrial O_2 consumption were zero order. The rate of respiration (k, in μM O_2 per minute) was thus the negative of the slope $d[O_2]/dt$. Cyanide markedly inhibited respiration, confirming that O_2 was consumed mainly by the mitochondrial respiratory chain.

For samples that were each run three times, the coefficient of variation of rates of respiration was <12%. NaCN inhibited respiration ≥96%.

Transmission electron microscopy

Samples were immersed in McDowell and Trump fixative for 3 hours at 25°C. Tissues were rinsed with phosphate-buffered saline and fixed with 1% osmium tetroxide for one hour. Samples were then washed with dH_2O, dehydrated in graded ethanol and propylene oxide, infiltrated, embedded in Agar 100 epoxy resin, and polymerized at 65°C for 24 hours. Blocks were trimmed, and semithin and ultrathin sections were cut using a Reichert Ultracuts ultramicrotome (Leica Microsystems GmbH, Wetzlar, Germany). The semithin (1 µm) sections were stained with 1% aqueous toluidine blue on glass slides. The ultrathin sections (95 nm) on 200 mesh copper grids were contrasted with uranyl acetate followed by a lead citrate double stain. The grids were examined and photographed under a Philips CM10 transmission electron microscope (TEM, Philips, Eindhoven, The Netherlands).

Results

MCM41-cal and SBA15-cal were synthesized using a surfactant supramolecular self-assembly method as described elsewhere.[18,19] The surfactant templates from the synthesized mesoporous materials were removed by heating the samples at 550°C for 6 hours under a flow of air in a temperature-programmable tube furnace. The resulting calcined materials were labeled as MCM41-cal and SBA15-cal. The synthesized MCM41-cal and SBA15-cal were then characterized by various methods, including nitrogen gas adsorption, elemental analysis, TEM, and solid-state nuclear magnetic resonance spectroscopy. The characterization results for MCM41-cal and SBA15-cal are summarized in Table 1. The surface area and pore diameters of MCM41-cal and SBA15-cal were determined by N_2 adsorption measurements (Figure 1). N_2 adsorption showed a type IV isotherm, indicating the presence of mesoporous silica. The surface area and average Barrett-Joyner-Halenda (BJH) pore diameter of MCM41-cal were found to be 1290 m^2/g and 28 Å, respectively, whereas the surface area and average BJH pore diameter of SBA15-cal was 955 m^2/g and 59 Å, respectively. TEM images of SBA15-cal and MCM41-cal are shown in Figure 1. The TEM images show that the MCM41-cal material consisted of spherical or oval-shaped microparticles with sizes in the range of 300–1000 nm, whereas the SBA15-cal material consisted of irregularly shaped and micron-sized particles about 1000 nm long and having typical diameters of approximately 500 nm.

The degree of condensation within the silica framework for MCM41-cal and SBA15-cal samples was determined using solid-state[28] Si{1H} cross-polarization magic angle spinning. The spectrum for SBA15-cal is depicted in Figure 1G, which shows well defined $(SiO)_2Si(OH)_2$ (Q^2), $(SiO)_3$-SiOH (Q^3), and $(SiO)_4$-Si (Q^4) silicate species, appearing at −94, −103, and −112 ppm, respectively.

Figure 2A–D shows the TEM micrographs of fetal blood mononuclear cells incubated with 500 µg/mL MCM41-cal particles for 2 hours. The number of MCM41-cal particles inside the cells was variable. Particles were seen inside the cytosol and engulfed by extended pseudopods. MCM41-cal was also seen in the cytosol of basophils without noticeable damage to the cellular organelles. MCM41-cal was seen in macrophages (Supplementary Figure 1A and B), neutrophil polymorphs (Supplementary Figure 1C–E), and lymphocytes (Supplementary Figure 1F). Particles were in the cytosol, either free (eg, Supplementary Figure 1E and F) or within vacuoles (eg, Supplementary Figure 1A). Some particles were attached to the plasma membrane (Supplementary Figure 1D–F), the nuclear membrane (with invaginations, Supplementary Figure 1B, C, and E), or the mitochondrial membrane (Supplementary Figure 1B–D).

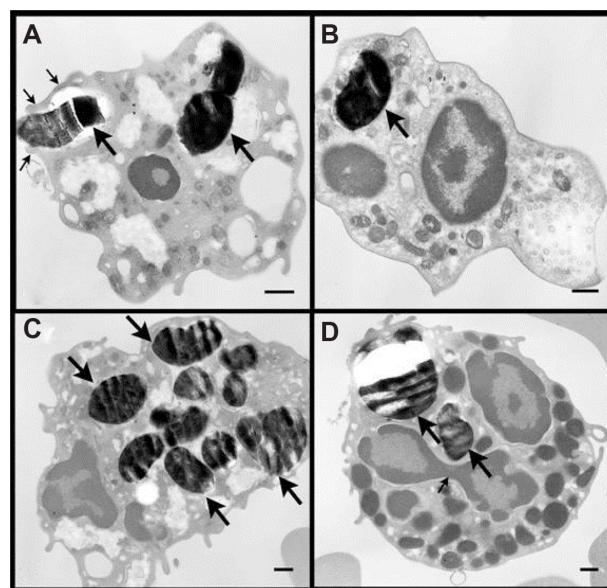TEM micrographs of fetal blood mononuclear cells incubated with 500 µg/mL SBA15-cal for 2 hours are shown in

Figure 2 Transmission electron microscopic images of fetal white blood cells incubated with 500 µg/mL MCM41-cal for 2 hours. The number of MCM41-cal (big arrows) inside the cells varied (Panels **A**–**D**). Panel **A** shows MCM41-cal inside the cytosol of a macrophage (large arrow) and another particle being engulfed by extended pseudopods (thin arrows). Panel **D** shows two MCM41-cal particles (big arrows) in the cytosol of a basophil; note the three lobes of the nucleus with a connecting strand (thin arrow) and large granules.
Note: Scale bar = 0.5 µm.

Figure 3A–D and Supplementary Figure 2. Many particles were seen within the cytosol of macrophages (big arrows in Figure 3A–C) or a neutrophil polymorphs (big arrows in Figure 3D) without obvious damage to any organelle (big arrows in Figure 3A–D). Many particles were seen in macrophages (Figure 3 and Supplementary Figure 2A–C) and neutrophil polymorphs (Supplementary Figure 2D). Particles were within vacuoles (Supplementary Figure 2A and D), attached to lysosomes (Supplementary Figure 2C), or near mitochondrial membranes (Supplementary Figure 2B).

Representative experiments for fetal mononuclear cell respiration in the presence and absence of MCM41-cal are shown in Figure 4A and B and of SBA15-cal in Figure 5A and B. In Figure 4A, fetal cells (9.6×10^7 cells/mL) were suspended in approximately 3 mL of phosphate-buffered saline, 10 mM glucose, 3 µM Pd phosphor, and 0.5% fat-free bovine serum albumin. The mixture was divided into two equal aliquots. MCM41-cal (0.5 mg/mL) was added to one aliquot with gentle stirring. The contents of each reaction were then transferred to a 1 mL size O$_2$ vial, which was sealed and placed in the instrument for O$_2$ measurement at 37°C.
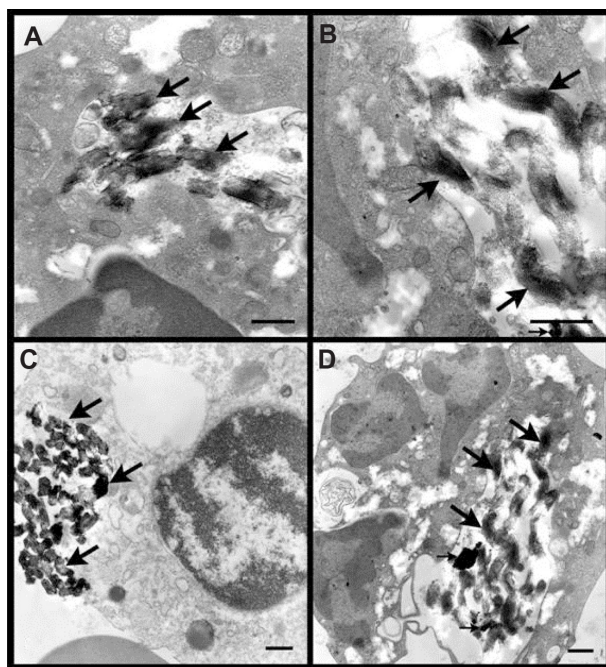

Figure 3 Transmission electron microscopic images of fetal blood mononuclear cells incubated with 500 µg/mL SBA15-cal for 2 hours. (**A**) Many SBA15-cal were seen within a vacuole in the cytosol of a macrophage without any obvious damage to any organelle (thick arrows). (**B**) Many SBA15-cal particles were seen within the cytosol of a macrophage and some of them were seen adherent to mitochondria without any obvious damage (thick arrow). (**C**) Many SBA15-cal were in the cytosol of a macrophage (thick arrow), in contact with a lysosome (thin arrow) without any evidence of phagosome-lysosome fusion. (**D**) Many SBA15-cal particles seen within a vacuole in the cytosol of a neutrophil polymorph, without any obvious damage to the organelles (thick arrows). Small arrows in (**C**) and (**D**) indicate artifacts.
Note: Scale bar = 0.5 µm.

The O$_2$ concentration was determined every 0.6 seconds. The two O$_2$ vials were alternated in the instrument every 5 minutes for a total of about 95 minutes. Thus, each [O$_2$] data point represented the mean ± standard deviation of approximately 3000 determinations. The rate of respiration (k, in µM O$_2$ per minute) was set as the negative of the slope of [O$_2$] versus t. The value of k (in µM O$_2$ per minute) for the untreated sample was 2.7 ($R^2 = 992$) and for the treated sample was 1.9 ($R^2 = 975$). In Figure 4B, fetal mononuclear cell (2.8×10^7 cells/mL) respiration was determined exactly as above. The value of k for the untreated sample was 1.8 ($R^2 = 996$) and for the treated sample was 1.7 ($R^2 = 996$). The results of a total of five independent experiments (expressed in µM O$_2$ per minute per 10^7 cells) are shown in Table 2. As shown, fetal cell respiration was unaffected by MCM41-cal ($P > 0.966$).

The same experiments were repeated with 0.5 mg/mL SBA15-cal. In Figure 5A, fetal mononuclear cell (7.2×10^7 cells/mL) respiration, determined exactly as above, was 3.8 µM O$_2$ per minute ($R^2 = 997$) for the untreated sample, and 3.7 µM O$_2$ per minute ($R^2 = 995$) for the treated sample. In Figure 5B, fetal mononuclear cell (18.3×10^7 cells/mL) respiration for the untreated sample was 5.4 µM O$_2$ per minute ($R^2 = 974$) and for the treated sample was 4.8 µM O$_2$ per minute ($R^2 = 988$). The results of a total of five independent experiments (expressed in µM O$_2$ per minute per 10^7 cells) are shown in Table 2. As shown, fetal cell respiration was unaffected by SBA15-cal ($P > 0.981$).

Additional results

TEM micrographs of fetal blood mononuclear cells incubated with 500 µg/mL MCM41-cal for 2 hours are shown in Supplementary Figure 1. No obvious damage to organelles was noted in any of the micrographs studied. MCM41-cal was seen in macrophages (Panels A and B), neutrophil polymorphs (Panels C–E), and lymphocytes (Panel F). Particles were seen in the cytosol, either free (eg, Panels E and F) or within vacuoles (eg, Panel A). Some particles were attached to the plasma membrane (Panels D–F), nuclear membrane (with clear invaginations, panels B, C, and E) and mitochondrial membrane (Panels B–D). There was an apparent attraction of MCM41-cal (eg, Supplementary Figure 1B) to the nuclear and mitochondrial membranes, a feature that could facilitate transferring particle contents to these organelles.

TEM micrographs of fetal blood mononuclear cells incubated with 500 µg/mL SBA15-cal for 2 hours are shown in Supplementary Figure 2. Similarly, no noticeable organelle damage was seen in any of the micrographs studied.
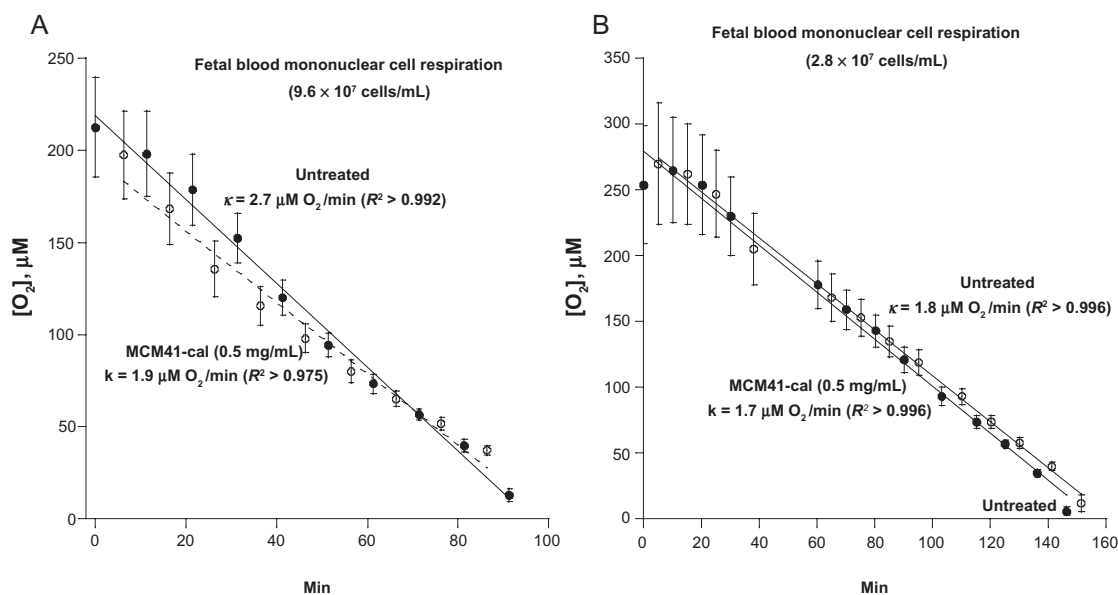
Figure 4 Representative experiments of fetal blood mononuclear cell respiration in the presence and absence of MCM41-cal.
Notes: All procedures were performed immediately following collection of venous blood from the umbilical cord. Respiration was measured in cells isolated from the whole blood with and without the addition of 0.5 mg/mL MCM41-cal. O_2 measurements were performed at 37°C in 1 mL sealed vials, alternating every 5 minutes between untreated (closed circles) and MCM41-cal (open circles) samples; each time point represents mean ± standard deviation (n = 1800) of $[O_2]$ over 3 minutes. The rate of respiration (k) was the negative of the slope of $[O_2]$ versus t; the values of k (in μM O_2 per minute) are shown. The lines are linear fits. Zero minutes corresponds to addition of particles.

Many SBA15-cal particles were seen in macrophages (Panels A–C) and neutrophil polymorphs (Panel D). Many particles were within vacuoles (Panels A and D) or attached to a lysosome (Panel C) or the mitochondrial membrane (Panel B). SBA15-cal was in contact with a lysosome without any evidence of phagosome-lysosome fusion (Supplementary Figure 2, Panel C). This phenomenon suggests a possible role for this type of particle in preventing this fusion, and could be beneficial from two points of view. In one view, it could inhibit lysosomal enzyme activation and consequent cell damage. In another view, inhibiting lysosomal enzymes could reduce damage to the particle contents.
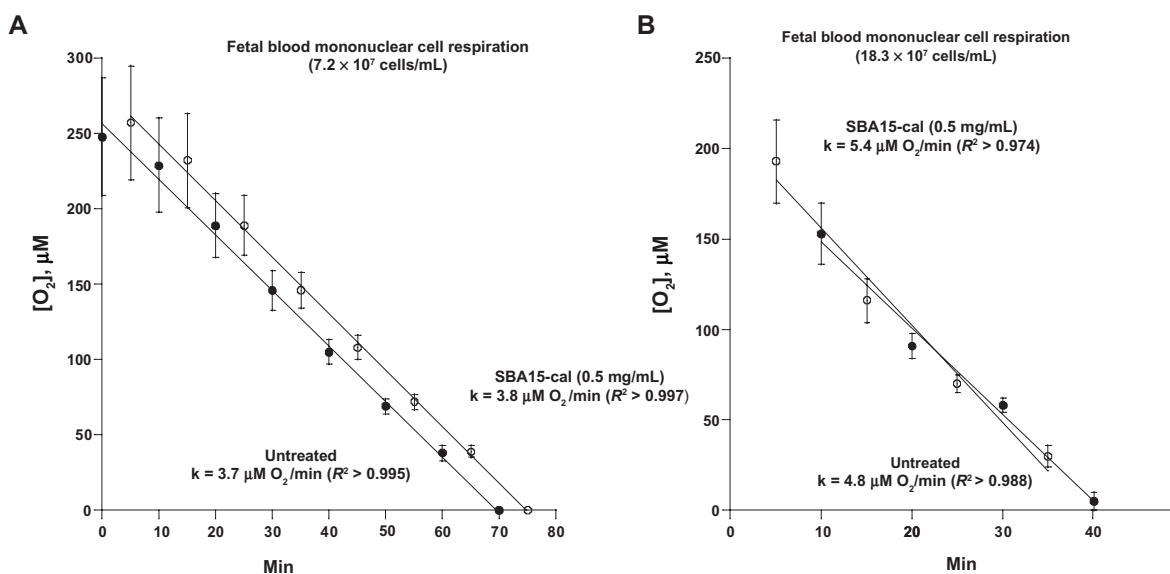

Figure 5 Representative experiments of fetal blood mononuclear cell respiration in the presence and absence of SBA15-cal.
Notes: All procedures were performed immediately following collection of venous blood from the umbilical cord. Respiration was measured in cells isolated from whole blood with and without the addition of 0.5 mg/mL SBA15-cal. O_2 measurements were performed at 37°C in 1 mL sealed vials, alternating every 5 minutes between untreated (closed circles) and SBA15-cal (open circles) samples; each time point represents the mean ± standard deviation (n = 1800) of $[O_2]$ over 3 minutes. The rate of respiration (k) was the negative of the slope of $[O_2]$ versus t; the values of k (in μM O_2 per minute) are shown. The lines are linear fits. Zero minutes corresponds to addition of particles.

Table 2 Respiration of fetal blood mononuclear cells with and without MCM41-cal or SBA15-cal

Rates of respiration (μM O$_2$ per minute per 10^7 cells)		
Untreated	**MCM41-cal**	**SBA15-cal**
0.42 ± 0.16 (n = 10)	0.39 ± 0.22 (n = 5)	0.44 ± 0.13 (n = 5)
	$P > 0.966$	$P > 0.981$

Discussion

Mesoporous silica nanomaterials and micromaterials have prospective clinical use for delivering bioactive compounds.[27] In this study, the biocompatibility of two forms of calcined mesoporous silica particles, ie, MCM41-cal and SBA15-cal, was investigated in fetal cells collected from umbilical cord blood. These micromaterials were prepared using different amphiphilic templates, ie, CTAB and Pluronic 123, respectively. MCM41-cal has a spherical or oval shape, whereas SBA15-cal has an irregular rod shape. In addition, MCM41 shows smaller lattice spacing and smaller BJH pore diameters (Figure 1 and Table 1). Despite these differences, both micromaterials have similar potential biological applications, as a result of their large surface areas, large pore volumes, microscale sizes, nanometer pores, and suitable properties for loading and delivering drugs, genes, and other bioactive molecules. Furthermore, calcined mesoporous silica particles are shown to be bioavailable and biocompatible.[22,23,28]

MCM41-cal and SBA15-cal were present inside fetal macrophages, neutrophils, and lymphocytes (Figures 2 and 3, and Figures S1 and S2). Their engulfment occurred without a need for surface activation by organic or polymeric groups, as previously reported for similar materials in other tissues.[9,10,20,29–31] Uptake was likely mediated by the high affinity of phospholipids in the plasma membrane for particle surface groups, such as silanols and silanolate.[25,32–34]

The TEM images (Figures 2 and 3, and Figures S1 and S2) show that MCM41-cal and SBA15-cal are distributed in different cellular compartments and are abundant in macrophages. They are also seen in different areas of the cytoplasm, suggesting intracellular movement. The particles do not appear to disturb cellular configuration or organelles. Some firmly attach to the nuclear membrane, seen as indentations. A similar observation of particles within the cytoplasm but not getting inside the nucleus has been reported in murine tissues[28] and in 3T3-L1 fibroblasts for chromophore-functionalized mesoporous materials.[27]

Particle aggregates are noted inside some fetal cells, especially for rod-shaped SBA15-cal. Particle aggregation in cellular cytosol for rod-shaped mesoporous silica (CTAB template

of about 450 nm size and aspect ratio of approximately 107 nm) has been previously reported.[35] Nevertheless, despite differences in shape, the results here show similar engulfment of MCM41-cal and SBA15-cal into fetal cells.

Compared with solvent-extracted particles, the calcined MCM41 and SBA15 used here have low-density surface silanols (as evident by ^{28}Si solid-state nuclear magnetic resonance spectroscopy). Thus, they are expected to generate fewer silanol-induced free radicals.[24–26] Moreover, absence of residual organics in the calcined materials (Table 1), due to the calcination procedure, might have contributed to their biocompatibility in fetal cells.

Another aim of this study was to investigate the biocompatibility of MCM41 and SBA15 with fetal blood cell bioenergetics, ie, cellular mitochondrial O$_2$ consumption. Recent studies have reported their safety in vitro,[23] but Hudson et al have described in vitro toxicity when using relatively high doses of MCM41 and SBA15 in mesothelial cells.[21]

Cellular mitochondrial oxygen consumption (respiration) implies delivery of O$_2$ and metabolic fuels to the mitochondria, oxidation of reduced metabolic fuels with release of electrons to O$_2$, and synthesis of adenosine triphosphate. Impaired respiration thus entails an interference with any of these processes.[22] Normal cellular respiration, on the other hand, implies well preserved glucose uptake and glycolysis, steady delivery of O$_2$ and metabolic fuels to the mitochondria, an intact mechanism and rate of oxidation of reduced metabolic fuels in the mitochondrial respiratory chain, normal passage of electrons to O$_2$, and coupled synthesis of adenosine triphosphate. Thus, the biochemical method and data are appropriate for assessing biocompatibility. The use of such cellular bioenergetics to assess nanoparticle and microparticle biocompatibility is discussed in more detail in our previous publications.[22,23,28] The results of our present work show that respiration in fetal mononuclear blood cells in the presence of MCM41-cal and SBA15-cal is similar to that of untreated cells, indicating reasonable biocompatibility between calcined mesoporous silica particles and fetal cellular bioenergetics (Table 2 and Figures 4 and 5).

The results show intact respiration (bioenergetics) of fetal blood cells treated with MCM41-cal or SBA15-cal for several hours. These findings are consistent with prior in vitro studies of biocompatibility of these two mesoporous silica particles in murine tissues.[23,28] This compatibility could be attributable to the refined method of particle preparation, including the lack of residual surfactant molecules as well as less density of surface silanols (Table 1). MCM41 and SBA15, with their amphiphilic templates extracted by solvent washing, were

not found to be biocompatible with lymphoid and myeloid hematopoietic cells.[22] These findings emphasize the impact of synthetic procedures on nanoparticle cytotoxicity and the need for careful assessment of the preparation protocols.

The biocompatibility of MCM41-cal and SBA15-cal in fetal blood cells is demonstrated here, primarily based on ultrastructure features and measurements of cellular bioenergetics,[23,36] but further studies using different fetal tissues and functional and structural methodologies are needed to confirm these preliminary results.

TEM studies are the gold standard for assessing ultrastructural changes, and the results of these analyses are consistent with the biochemical (functional) data described earlier. The TEM images also clearly show abundant internalization of the particles inside cells, along with well preserved organelles.

It is worth noting that, despite their different sizes (Table 1), the two silica particles used here showed the same degree of biocompatibility. Unlike with traditional materials, findings with regard to biocompatibility of nanomaterials and micromaterials are difficult to generalize and require particle-specific investigation. This stems from the fact that composition, size, shape, surface charge, surface properties (hydrophilicity versus hydrophobicity), residual materials, method of preparation, and other structural features all impact biological properties and thus biocompatibility and cytotoxicity.

Among various structural and compositional factors, the size of nanomaterials and micromaterials plays a critical role. The impact of two different sizes of silica nanotubes on normal and cancer cells has been investigated. Particle size was found to influence both uptake and cytotoxicity. At the same concentration, 200 nm nanotubes were more toxic than 500 nm nanotubes.[37] Size-dependent neurotoxicity of copper nanomaterials (40–80 nm) was demonstrated in murine somatosensory neurons, with smaller particles being more toxic than larger ones.[38]

The cytotoxicity of nanosized and microsized CuO materials was studied in a human alveolar cell line.[39] The 42 nm particles were significantly more toxic to the mitochondria and DNA than were the 3 µm particles. However, the same study also showed that Fe_2O_3 (<1 µm) and TiO_2 (1 µm) particles caused more DNA damage than their corresponding nanoparticles (29 nm and 63 nm, respectively). Thus, it is reasonable to conclude that the biological effects of particles are influenced by numerous variables including size, composition, and host cells.

In summary, this study suggests that MCM41-cal and SBA15-cal are reasonably biocompatible with fetal mononuclear blood cells. The results are consistent with other studies using cell culture or in vivo systems with longer exposure times.[2] The results also show well preserved mononuclear blood cell structure (by electron microscopy) and function (by cellular respiration) after treatment with either type of material, confirming biocompatibility. The benign properties of MCM41-cal and SBA15-cal are likely due to the refined methods of synthesis and calcination, resulting in fewer surface hydroxyl groups and free residual surfactants (as evident by the solid-state nuclear magnetic resonance data).

Acknowledgments

Disclosure

The authors report no conflicts of interest in this work.

References

1. Kipen HM, Laskin DL. Smaller is not always better: nanotechnology yields nanotoxicology. *Am J Physiol Lung Cell Mol Physiol*. 2005;289(5): L696–L708.
2. Nel A, Xia T, Madler L, Li N. Toxic potential of materials at the nanolevel. *Science*. 2006;311(5761):622–627.
3. Bottini M, Bruckner S, Nika K, et al. Multi-walled carbon nanotubes induce T lymphocyte apoptosis. *Toxicol Lett*. 2006;160(2):121–126.
4. Lin W, Huang YW, Zhou XD, Ma Y. In vitro toxicity of silica nanoparticles in human lung cancer cells. *Toxicol Appl Pharmacol*. 2006;217(3):252–259.
5. Sayes CM, Gobin AM, Ausman KD, Mendez J, West JL, Colvin VL. Nano-C60 cytotoxicity is due to lipid peroxidation. *Biomaterials*. 2005;26(36):7587–7595.
6. Slowing I, Trewyn BG, Lin VS. Effect of surface functionalization of MCM-41-type mesoporous silica nanoparticles on the endocytosis by human cancer cells. *J Am Chem Soc*. 2006;128(46):14792–14793.
7. Di Pasqua AJ, Sharma KK, Shi YL, et al. Cytotoxicity of mesoporous silica nanomaterials. *J Inorg Biochem*. 2008;102(7):1416–1423.
8. Hessler JA, Budor A, Putchakayala K, et al. Atomic force microscopy study of early morphological changes during apoptosis. *Langmuir*. 2005;21(20):9280–9286.
9. Rosenholm JM, Peuhu E, Eriksson JE, Sahlgren C, Linden M. Targeted intracellular delivery of hydrophobic agents using mesoporous hybrid silica nanoparticles as carrier systems. *Nano Lett*. 2009;9(9):3308–3311.
10. Xia T, Kovochich M, Liong M, et al. Polyethyleneimine coating enhances the cellular uptake of mesoporous silica nanoparticles and allows safe delivery of siRNA and DNA constructs. *ACS Nano*. 2009;3(10):3273–3786.
11. Rosenholm JM, Peuhu E, Bate-Eya LT, Eriksson JE, Sahlgren C, Linden M. Cancer-cell-specific induction of apoptosis using mesoporous silica nanoparticles as drug-delivery vectors. *Small*. 2010;6(11):1234–1241.
12. Vallet-Regi M, Balas F, Arcos D. Mesoporous materials for drug delivery. *Angew Chem Int Ed Engl*. 2007;46(40):7548–7558.
13. Lu J, Liong M, Sherman S, et al. Mesoporous silica nanoparticles for cancer therapy: energy-dependent cellular uptake and delivery of Paclitaxel to cancer cells. *Nanobiotechnology*. 2007;3(2):89–95.

14. Slowing II, Trewyn BG, Lin VSY. Mesoporous silica nanoparticles for intracellular delivery of membrane-impermeable proteins. *J Am Chem Soc*. 2007;129(28):8845–8849.

15. Liong M, Lu J, Kovochich M, et al. Multifunctional inorganic nanoparticles for imaging, targeting, and drug delivery. *ACS Nano*. 2008;2(5):889–8896.

16. Rosenholm JM, Meinander A, Peuhu E, et al. Targeting of porous hybrid silica nanoparticles to cancer cells. *ACS Nano*. 2009;3(1):197–206.

17. Hom C, Lu J, Liong M, et al. Mesoporous silica nanoparticles facilitate delivery of siRNA to shutdown signaling pathways in mammalian cells. *Small*. 2010;6(11):1185–1190.

18. Kresge CT, Leonowicz ME, Roth WJ, Vartuli JC, Beck JS. Ordered mesoporous molecular sieves synthesized by a liquid-crystal template mechanism. *Nature*. 1992;359(6397):710–712.

19. Zhao D, Feng J, Huo Q, et al. Triblock copolymer syntheses of mesoporous silica with periodic 50–300 angstrom pores. *Science*. 1998;279(5350):548–552.

20. Blumen SR, Cheng K, Ramos-Nino ME, et al. Unique uptake of acid-prepared mesoporous spheres by lung epithelial and mesothelioma cells. *Am J Respir Cell Mol Biol*. 2007;36(3):333–342.

21. Hudson SP, Padera RF, Langer R, Kohane DS. The biocompatibility of mesoporous silicates. *Biomaterials*. 2008;29(30):4045–4055.

22. Tao Z, Morrow MP, Asefa T, et al. Mesoporous silica nanoparticles inhibit cellular respiration. *Nano Lett*. 2008;8(5):1517–1526.

23. Al Shamsi M, Al Samri MT, Al-Salam S, et al. Biocompatibility of calcined mesoporous silica particles with cellular bioenergetics in murine tissues. *Chem Res Toxicol*. 2011;23(11):1796–1805.

24. Konecny R, Leonard S, Shi X, Robinson V, Castranova V. Reactivity of free radicals on hydroxylated quartz surface and its implications for pathogenicity experimental and quantum mechanical study. *J Environ Pathol Toxicol Oncol*. 2001;20 Suppl 1:119–132.

25. Murashov V, Harper M, Demchuk E. Impact of silanol surface density on the toxicity of silica aerosols measured by erythrocyte haemolysis. *J Occup Environ Hyg*. 2006;3(12):718–723.

26. Johnston AP, Battersby BJ, Lawrie GA, Trau M. Porous functionalised silica particles: a potential platform for biomolecular screening. *Chem Commun (Camb)*. 2005;21(7):848–850.

27. Lin YS, Tsai CP, Huang HY, et al. Well-ordered mesoporous silica nanoparticles as cell markers. *Chem Mater*. 2005;17(18):4570–4573.

28. Al-Salam S, Balhaj G, Al-Hammadi S, et al. In vitro study and biocompatibility of calcined mesoporous silica microparticles in mouse lung. *Toxicol Sci*. 2011;122(1):86–99.

29. Beyerle A, Irmler M, Beckers J, Kissel T, Stoeger T. Toxicity pathway focused gene expression profiling of PEI-based polymers for pulmonary applications. *Mol Pharm*. 2012;7(3):727–737.

30. Galagudza MM, Korolev DV, Sonin DL, et al. Targeted drug delivery into reversibly injured myocardium with silica nanoparticles: surface functionalization, natural biodistribution, and acute toxicity. *Int J Nanomedicine*. 2010;5:231–237.

31. Radu DR, Lai CY, Jeftinija K, Rowe EW, Jeftinija S, Lin VS. A polyami-doamine dendrimer-capped mesoporous silica nanosphere-based gene transfection reagent. *J Am Chem Soc*. 2004;126(41):13216–13217.

32. Allison AC, Harington JS, Birbeck M. An examination of the cytotoxic effects of silica on macrophages. *J Exp Med*. 1966;124(2):141–154.

33. Chunbo Y, Daqing Z, Aizhuo L, Jiazuan N. A NMR study of the interaction of silica with dipalmitoylphosphatidylcholine liposomes. *J Colloid Interface Sci*. 1995;172(2):536–538.

34. Murashov VV, Leszczynski J. Adsorption of the phosphate groups on silica hydroxyls: an initio study. *J Phys Chem A*. 1999;103(9): 1228–1238.

35. Tsai CP, Hung Y, Chou YH, et al. High-contrast paramagnetic fluorescent mesoporous silica nanorods as a multifunctional cell-imaging probe. *Small*. 2008;4(2):186–191.

36. Al Samri MT, Al Shamsi M, Al Salam S, et al. Measurement of oxygen consumption by murine tissues in vitro. *J Pharmacol Toxicol Methods*. 2011;63(2):196–204.

37. Nan A, Bai X, Son SJ, Lee SB, Ghandehari H. Cellular uptake and cytotoxicity of silica nanotubes. *Nano Lett*. 2008;8(8):2150–2154.

38. Prabhu BM, Ali SF, Murdock RC, Hussain SM, Srivatsan M. Copper nanoparticles exert size and concentration dependent toxicity on soma-tosensory neurons of rat. *Nanotoxicology*. 2010;4(2):150–160.

39. Karlsson HL, Gustafsson J, Cronholm P, Möller L. Size-dependent toxicity of metal oxide particles – a comparison between nano- and micrometer size. *Toxicol Lett*. 2009;188(2):112–118.
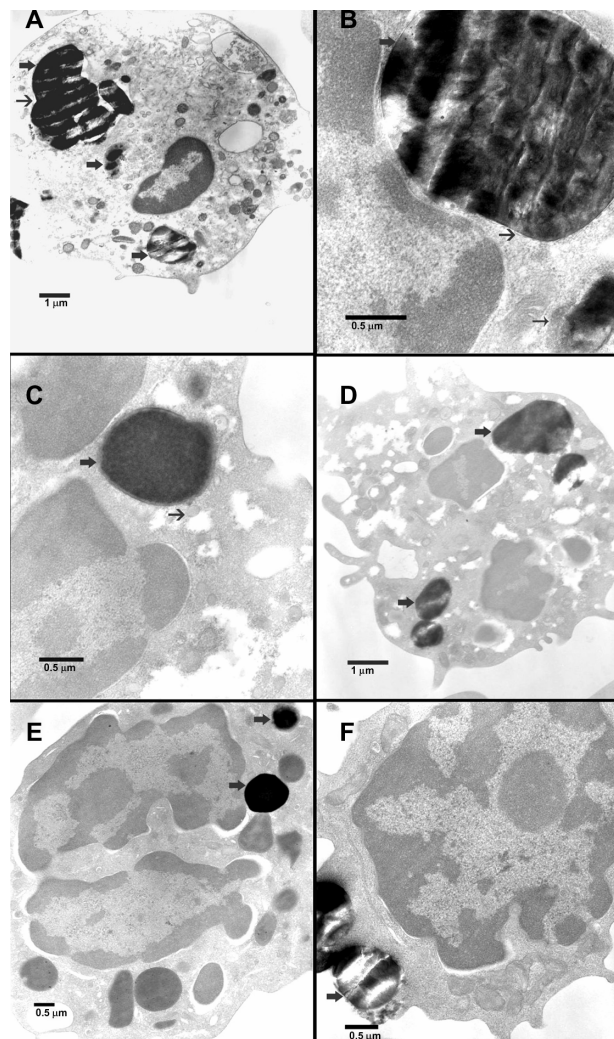
Supplementary figures

Figure S1 Transmission electron microscopic images of fetal blood mononuclear cells incubated with 500 µg/mL MCM41-cal for 2 hours. (**A**) MCM41-cal particles were seen within vacuoles (thick arrows), in the cytosol of a macrophage, not obviously attached to any organelle. (**B**) MCM41-cal was seen within a vacuole (thin arrow) and strictly attached to the nuclear membrane of a macrophage with clear invagination of the nuclear membrane in the area of adherence without obvious damage (thick arrow), another MCM41-cal was seen adherent to a mitochondrion without any obvious damage (thin arrow). (**C**) MCM41-cal was in a neutrophil polymorph, within a vacuole (thick arrow), adhering to the nucleus and mitochondria (thin arrow) without causing any obvious damage. (**D**) MCM41-cal particles were in the cytosol of a neutrophil polymorph, within vacuoles and close to mitochondria (thick arrow). (**E**) MCM41-cal was seen in the cytosol of a neutrophil polymorph closely adhering to the nucleus (thick arrow) and another particle was seen passing the cell membrane without any obvious damage (thick arrow). (**F**) Two MCM41-cal particles were seen in the cytosol of a lymphocyte after crossing the cell membrane without any obvious damage (thick arrow).
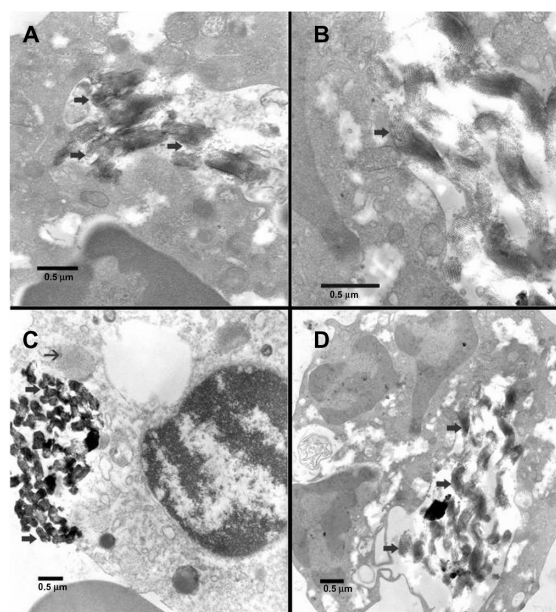

Figure S2 Transmission electron microscopic images of fetal blood mononuclear cells incubated with 500 µg/mL SBA15-cal for 2 hours. (**A**) Many SBA15-cal were seen within a vacuole in the cytosol of a macrophage without any obvious damage to any organelle (thick arrows). (**B**) Many SBA15-cal particles were seen within the cytosol of a macrophage and some of them were seen adherent to mitochondria without any obvious damage (thick arrow). (**C**) Many SBA15-cal were in the cytosol of a macrophage (thick arrow), in contact with a lysosome (thin arrow) without any evidence of phagosome-lysosome fusion. (**D**) Many SBA15-cal particles were within a vacuole in the cytosol of a neutrophil polymorph without any obvious damage to the organelles (thick arrows).